NANO · MICRO small
www.small-journal.com

Rolling up $MoSe_2$ Nanomembranes as a Sensitive Tubular Photodetector

*Xuefei Zhou, Ziao Tian, Hyuk Jin Kim, Yang Wang, Borui Xu, Ruobing Pan, Young Jun Chang, Zengfeng Di, Peng Zhou, and Yongfeng Mei**

Transition metal dichalcogenides, as a kind of 2D material, are suitable for near-infrared to visible photodetection owing to the bandgaps ranging from 1.0 to 2.0 eV. However, limited light absorption restricts photoresponsivity due to the ultrathin thickness of 2D materials. 3D tubular structures offer a solution to solve the problem because of the light trapping effect which can enhance optical absorption. In this work, thanks to mechanical flexibility of 2D materials, self-rolled-up technology is applied to build up a 3D tubular structure and a tubular photodetector is realized based on the rolled-up molybdenum diselenide microtube. The tubular device is shown to present one order higher photosensitivity compared with planar counterparts. Enhanced optical absorption arising from the multiple reflections inside the tube is the main reason for the increased photocurrent. This tubular device offers a new design for increasing the efficiency of transition metal dichalcogenide–based photodetection and could hold great potential in the field of 3D optoelectronics.

Transition metal dichalcogenides (TMDCs) are a kind of 2D materials which attract much attention in last decade because of their superior optical and electrical properties as well as potential applications.[1–8] Unlike graphene, semiconductor TMDCs have sizable bandgaps ranging from 1.0 to 2.0 eV which is located in the near-infrared and visible region.[9] Bandgaps in TMDCs are tunable by applying external electric field or mechanical strain. Combined with broad-band optical absorption and mechanical flexibility, TMDCs are one of appealing materials for the application in optoelectronic devices such as field effect transistors, photodetectors, and light-emitting diodes. Photodetectors based on molybdenum disulfide (MoS_2),[1,3] tungsten disulfide (WS_2),[10,11] molybdenum diselenide ($MoSe_2$),[7,8] and their heterojunctions[12] were constructed and exhibited photoresponsivity ranging from a few mA W^{-1} to several hundred A W^{-1}, which is related to the materials selected, layer numbers, and device contacts. Intrinsically, the photoresponsivity is restricted by their absorption cross section and present lower values because of small thickness of TMDCs.[9] Integration of TMDC materials into photonic structures such as photonic crystals and microcavities offers a solution to enhance the photoresponsivity.[13–15] For example, Fano-resonant photonic crystals could significantly boost light absorption in monolayer MoS_2 and the absorption can reach up to 90% at the resonant wavelength.[13] Another typical approach to enhancing photoresponsivity is to hybridize TMDCs with plasmonic structures. A MoS_2 photodetector hybridized with Ag nanowire network was demonstrated and presented greatly enhanced photocurrent over the pristine MoS_2 photodetectors because of surface plasmon coupling.[5] However, the photoresponsivity can be only enhanced at designed and selected wavelength in these hybrid photodetectors mentioned above. It is promising that 3D mesostructures could enhance light absorption over wide range due to its circular geometry and thus improve photoelectric performance.[16–19]

Rolled-up inorganic nanomembrane–based 3D architectures,[20–22] such as nanoscrolls and nanosprings, have great potential in applications of supercapacitors,[23] optical microcavity,[24–26] actuators,[27,28] resistive random access memory,[29] motors,[30] etc., because of their distinct properties arising from 3D geometry. In this work, a 3D tubular photodetector is proposed to increase the photoresponsivity of 2D materials benefiting from the significantly enhanced light absorption. We introduce this tubular microstructure into the $MoSe_2$-based photodetector for improved detection performance. 3D photodetector based on rolled-up $MoSe_2$ nanomembrane was

X. F. Zhou, Y. Wang, Dr. B. R. Xu, R. B. Pan, Prof. Y. F. Mei
Department of Materials Science and State Key Laboratory of ASIC and system
Fudan University
Shanghai 200433, P. R. China
E-mail: yfm@fudan.edu.cn
Prof. Z. A. Tian, Prof. Z. F. Di
State Key Laboratory of Functional Materials for Informatics
Shanghai Institute of Microsystem and Information Technology
Chinese Academy of Sciences
Shanghai 200050, P. R. China
H. J. Kim, Prof. Y. J. Chang
Department of Physics
University of Seoul
Seoul 02504, Republic of Korea
Prof. P. Zhou
State Key Laboratory of ASIC and System
School of Microelectronics
Fudan University
Shanghai 200433, P. R. China
The ORCID identification number(s) for the author(s) of this article can be found under https://doi.org/10.1002/smll.201902528.

DOI: 10.1002/smll.201902528

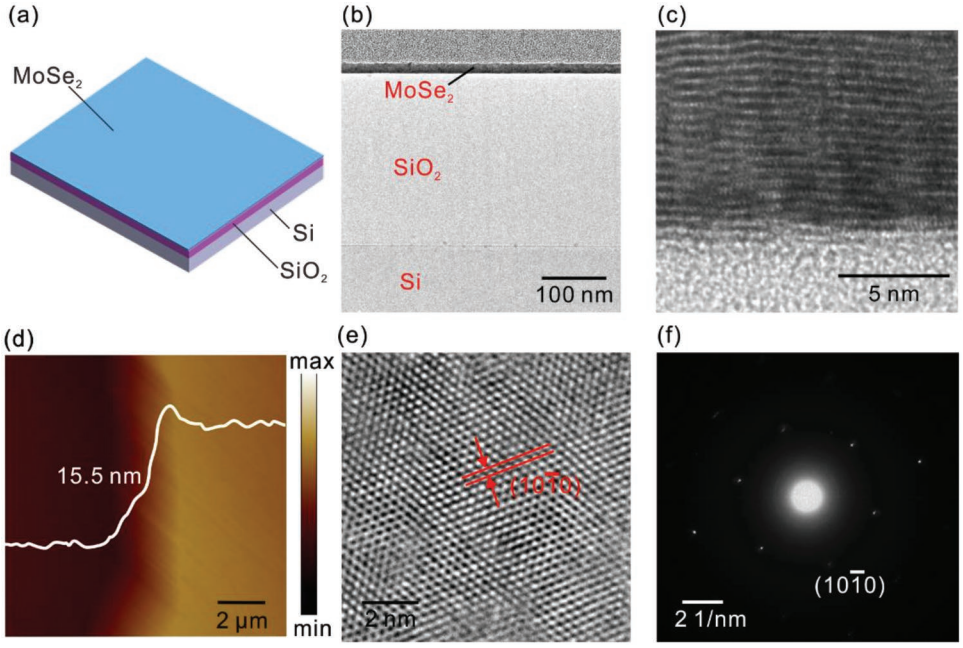

Figure 1. a) Schematic diagram of $MoSe_2$ nanomembrane deposited on Si/SiO_2 substrate. b) TEM image of the cross section of $MoSe_2$ sample. c) High-magnification TEM image of $MoSe_2$ layer. d) AFM image of unprocessed $MoSe_2$ membrane and the flake thickness determined by topographic analysis. e,f) HRTEM image of a dispersed $MoSe_2$ flake and corresponding SAED pattern.

constructed via self-rolled-up technology. Such $MoSe_2$-based 3D photodetector exhibits superior (one order higher) photosensitivity compared with its planar device. Except from improved light absorption, the enhancement also comes from reduced dark current, which is due to the increased surface state density and bandgap modification of strained $MoSe_2$ nanomembranes. The tubular photodetector proposed has great potential for integration of 3D optoelectronics and is capable to be applied in wide angle detection.

The fabrication of rolled-up tubular $MoSe_2$ photodetector is started with an ultrathin $MoSe_2$ nanomembrane grown on silicon substrate with covered SiO_2 layer (**Figure 1**a). $MoSe_2$ nanomembrane was deposited on SiO_2/Si substrate at 260 °C by high-vacuum coevaporation. Target materials Mo and Se were separately heated by e-beam and thermal evaporation at the rates of 0.1 and 1 Å s^{-1}, respectively.[31] A cross-sectional scanning transmission electron microscopy (TEM) image illustrating the heterostructure stack is shown in Figure 1b. Different layers are clearly distinguished from each other. The structural and morphological properties of the ultrathin $MoSe_2$ nanomembranes were investigated by higher magnification TEM image as shown in Figure 1c, which depicts clear boundary and layered structure, illustrating good quality of the $MoSe_2$ nanomembranes. In order to explore the thickness of $MoSe_2$ nanomembrane, the atomic force microscopy (AFM) image was measured. As plotted in Figure 1d, the height difference between the membrane and the substrate exhibits that the thickness of our membrane is about 15.5 nm. Figure 1e displays an in-plane high-resolution TEM (HRTEM) image of a dispersed $MoSe_2$ flake, in which the lattice spacing is measured to be 0.28 nm, corresponding to the $\{10\bar{1}0\}$ planes. A hexagonal structure of $MoSe_2$ was also observed in HRTEM image and further confirmed by selected area electron diffraction (SAED) pattern (Figure 1f), which exhibits a set of sixfold symmetry diffraction spots, coincident with other works.[4,7,32]

The $MoSe_2$ microtubes were fabricated through self-rolled-up technique, microfabrication process of which is schematically illustrated in **Figure 2**a–c. First, photolithography and reactive ion beam (RIE) etching were utilized to pattern the $MoSe_2$ nanomembrane as depicted in Figure 2a. A U shape corrosion window was formed, where SiO_2 layer was exposed to the air. Then, second photolithography was adopted to define the electrode areas and channel size of the tubular device. After that, a strained layer of chromium (Cr, 20 nm) and platinum (Pt, 5 nm) was deposited on $MoSe_2$ nanomembranes by e-beam evaporation system. Notably, the Cr/Pt layer plays two roles in the fabrication process. It serves as not only the strained layer for rolling up process but also the electrodes of tubular device. After lift-off of photoresist, device based on planar $MoSe_2$ nanomembrane was constructed, with the channel length of 16 μm, as shown in Figure 2b (sketched image). Subsequently, silicon dioxides layer was selectively etched by 40% hydrogen fluoride (HF) solution. $MoSe_2/Cr/Pt$ layers were released from substrate and rolled up to a tubular structure driven by the stress difference in the multilayers (Figure 2c). The array of rolled-up $MoSe_2$ microtubes is displayed in Figure 2d. Measured from this scanning electron microscopy (SEM) image, the diameter of these microtubes is about 6.2 μm and could be tuned by the top Cr layer. Figure 2e depicts the magnified SEM image of one of microtubes in the array (red dashed box). The side view of this microtube (blue dashed box) is displayed in Figure 2f, from which we can distinctly observe the opening of the tubular structure. Compared with previously reported methods of rolling up TMDCs flakes,[33,34] this kind of method has distinct advantages in adjusting the diameter of microtube by controlling the induced stress during the growth progress

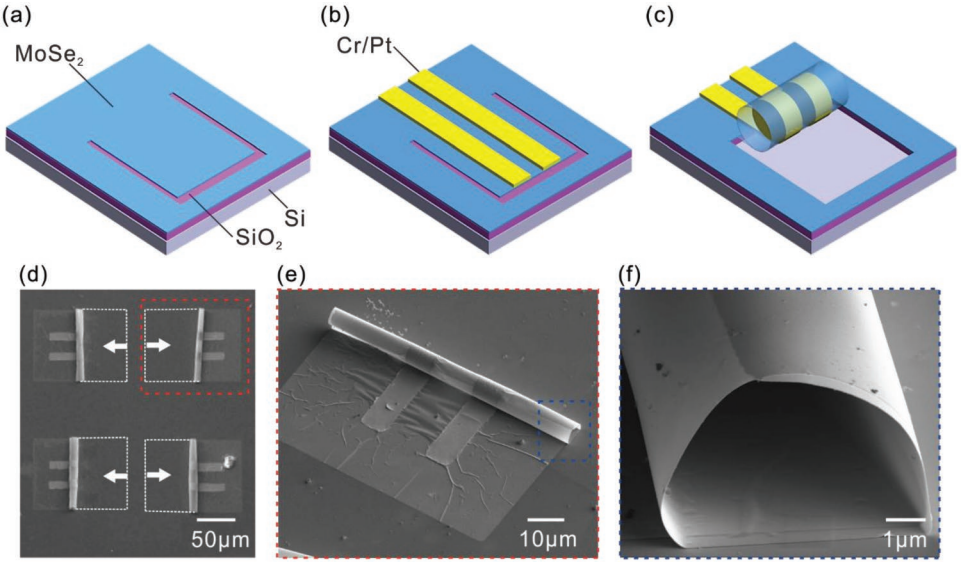

Figure 2. a–c) 3D schematic view of the fabrication process of roll-up $MoSe_2$ microtube. SEM images of rolled-up $MoSe_2$ microtubes: d) Array of microtubes. e) Focused view of a single microtube. f) Side view of the microtube.

of stress layer.[35] Moreover, device size such as channel length can be easily designed in the step of photolithography. In our method, the position of the tubular device is controllable and the devices were fabricated on chip. Thus, it is more suitable for the fabrication of device arrays and on-chip integration. What is more, our method is a versatile technique to fabricate different TMDCs microtubes.

In order to investigate the electrical properties of the tubular device, after the rolling-up process and characterization, *I–V* characteristics of the tubular device were measured by semiconductor parameter analyzer at room temperature. Counterparts of unreleased $MoSe_2$ nanomembrane–based planar device had been characterized for comparison before rolling-up process. The optical microscopy images of the device before and after rolling-up process are depicted in **Figure 3**a,b, respectively. In the planar device, the channel area is 30 μm × 120 μm and both electrodes are 28 μm in width. After rolling-up, the diameter of the $MoSe_2$ microtube is around 30.5 μm. These parameters can be adjusted during the fabrication progress as we mentioned before. As shown in Figure 3c, current in tubular device declines compared with that of planar device. At a bias voltage of 2 V, the current of the planar device is 1.13×10^{-4} A, while that of tubular device is 6.03×10^{-5} A. The current of the tubular device is nearly a half compared with that of the planar device. The reasons for the decrease of current in the tubular device will be discussed later.

As a photodetector, one of the most important characteristics is the response to light. To explore photoelectric properties of planar device and tubular device, an 808 nm laser beam was used for irradiation as schematically displayed in **Figure 4**a,b (the inset in the left bottom corner). Figure 4a,b respectively shows the measured *I–V* characteristics of the planar and tubular devices in the presence of an illuminating laser with different power densities (P_{inc}) ranging from 20.0 to 443.1 mW cm^{-2}. In both devices, current increases with the increase of laser power density at a fixed bias. As schematically illustrated in the inset of Figure 4c, under illumination, electron–hole pairs are generated and can be extracted by applying a drain-source bias. A larger laser power could lead to the increased number of photon-generated carriers, consequently, photocurrent increases.[2,3,6,8] Figure 4c depicts photocurrent (I_{ph}) as a function of incident optical power density. We can find that photocurrent of the tubular device is enhanced in comparison with that of planar device at the same incident optical power density. Photoresponsivity (*R*) and photodetectivity (*D**) are two key figures-of-merit of

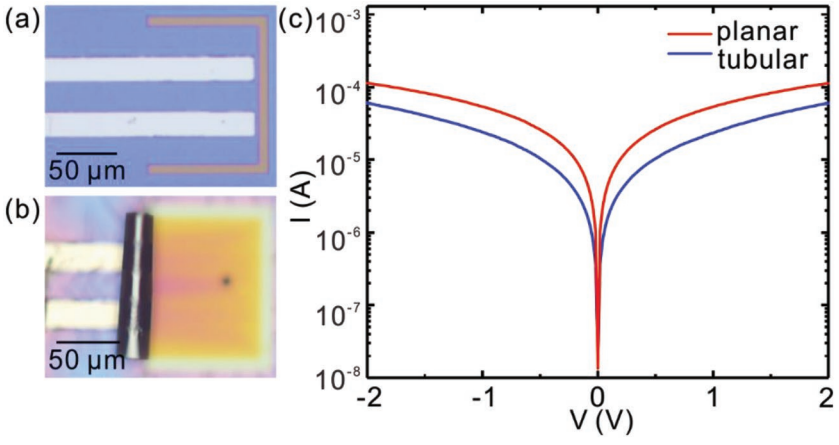

Figure 3. a,b) Optical images of $MoSe_2$ device before and after the rolling-up process. c) *I–V* characteristics of the tubular and planar device.

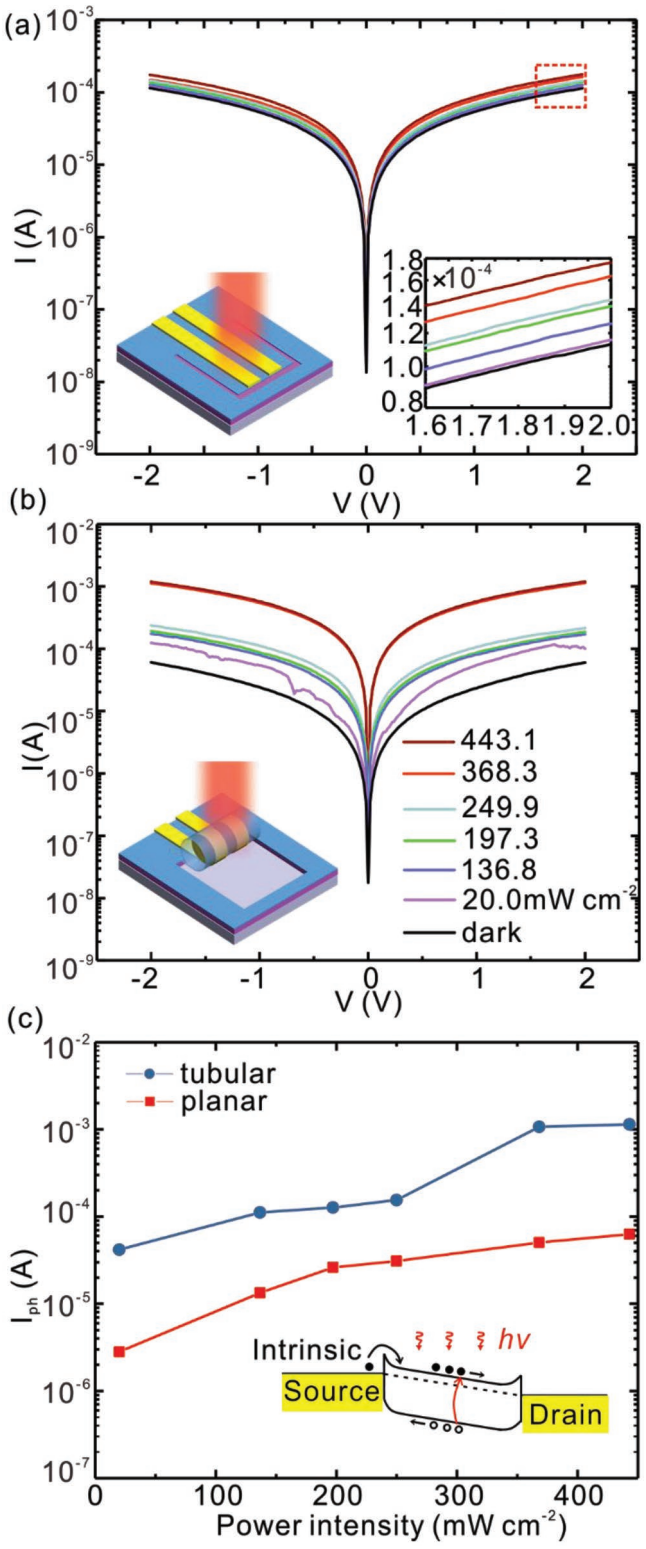

Figure 4. *I–V* characteristics of a) planar, b) tubular devices in the dark and in the presence of an illumination laser (power density ranging from 20.0 to 443.1 mW cm^{-2}). c) Photocurrent as a function of incident optical power density. (Inset: band diagram of the $MoSe_2$ photodetector device).

a photodetector. R is defined as the ratio of photocurrent to the incident power, which is given by Equation (1)

$$R = \frac{I_{ph}}{P} = \frac{I_{light} - I_{dark}}{P} \quad (1)$$

where I_{ph} is the photocurrent, I_{light} is the current measured under the light illumination, I_{dark} is the dark current, and P is the incident laser power . D^* represents the ability to detect signal from the noise and is defined as

$$D^* = \frac{RA^{1/2}}{(2eI_{dark})^{1/2}} \quad (2)$$

where A *is* the effective area of the photodetector, e is the absolute value of electron charge, and I_{dark} is the dark current. Based on the above equations, the R and D^* of tubular device are calculated to be 282.5 A W^{-1} and 1.96×10^{11} Jones under the illumination of 808 nm light (368.3 mW cm^{-2}), respectively. **Figure 5**a plots the R and D^* of the tubular device as a function of light power intensity, which is dozens of times larger than the corresponding planar device (Figure S3a, Supporting Information), as a result of the higher photocurrent and decreased device area. Moreover, under the same conditions, photosensitivity, another important parameter to evaluate the performance of photodetector, which is defined as the ratio of photocurrent-to-dark-current (PDR), given by $PDR = \frac{I_{ph}}{I_{dark}}$, is distinctly enhanced in the tubular photodetector compared with the planar device ($PDR_{tubular}$ = 19, PDR_{planar} = 0.45). To analyze the stability of our tubular photodetector, we investigated the time-resolved photoresponse of the device. Figure 5b shows the current of the device as a function of time at a bias voltage of 2 V and power intensity of 368.3 mW cm^{-2}. The device exhibits a repeatable and stable response to the light illumination.

Next, we want to investigate the reasons for the decrease of dark current and the increase of photocurrent in the tubular device compared with those in planar device. Considering the structure difference between the planar and tubular device, we propose three reasons for the different photosensitivity: 1) change of bandgap, 2) higher surface state density, and 3) enhanced optical absorption.

The energy band of $MoSe_2$ can be affected by strain of the membrane. Strain engineering is a promising method to tune the band structure and thus influence optical and electronic properties of transition metal dichalcogenides. For example, S. B. Desai et al. have demonstrated that multilayer WSe_2 will experience an indirect-to-direct bandgap transition with the increasing applied strain. The transition is attributed to the decrease of direct bandgap (K_C–K_V) and the increase of indirect bandgap (Σ–K_V).[36] Y. Sun et al. calculated the band structure evolution of bilayer $MoSe_2$ under the tensile strain through first-principle calculation and found that the indirect bandgap increases by applying tensile strain.[37] Previous studies have proved that strain can be introduced into the curved films due to the curvature effect.[38,39] Raman spectra has proven to be a powerful tool to characterize 2D TMDCs samples subjected to uniaxial strain.[40–42] Here, we study the vibrational modes change in the rolled-up $MoSe_2$ microtube by Raman spectroscopy as shown in **Figure 6**a (the excitation laser wavelength is 514 nm). Figure 6a is Raman spectrum of 15.5 nm $MoSe_2$

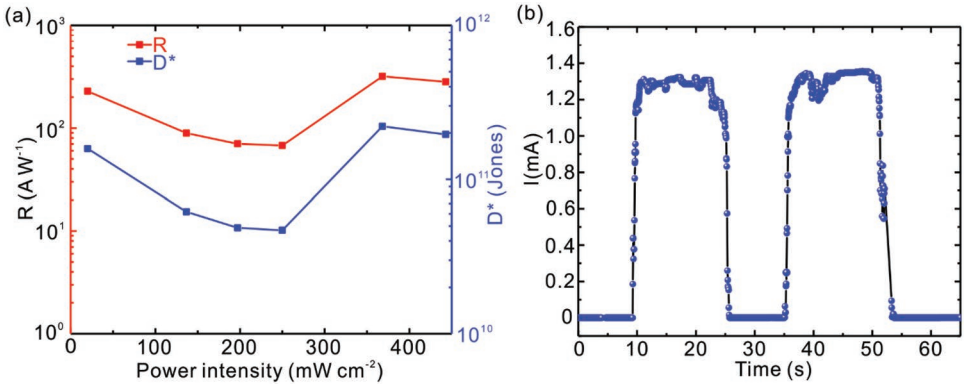

Figure 5. a) Power intensity-dependent photoresponsivity (*R*) and photodetectivity (*D**) and b) time-resolved photoresponse of the tubular photodetector at a bias voltage of 2 V and a laser power intensity of 368.3 mW cm^{-2}.

membrane before (red line) and after (blue line) the rolling-up process. As shown in the figure, A_{1g} mode of $MoSe_2$ microtube is redshifted with 2.26 cm^{-1} wavenumber difference compared with unprocessed planar membrane, which is attributed to the strain induced by the tubular structure. The uniaxial shift $\Delta\omega_{A1g}$ can be expressed as[42,43]

$$\Delta\omega_{A1g} = -2\omega^0_{A1g}\,\gamma_{A1g}\varepsilon \tag{3}$$

where γ_{A1g} is Gruneisen parameter and ε represents uniaxial strain. The mode shift is proportional to uniaxial strain. According to the theoretical calculation and experimental results reported before, A_{1g} mode shifts to lower frequency at a rate of –6.97 cm^{-1} per % strain in the small strain range.[44] Thus, the strain of the tubular $MoSe_2$ nanomembrane is calculated to be ≈0.32%, which is consistent with other works on curvature effect.[26] Under small uniaxial tensile strain, the indirect bandgap increases slightly[36] which is mostly on account of the increase of the energy of the conduction band minima at Σ point and thus the Schottky barrier between the metal–semiconductor interface increases as schematically illustrated in Figure 6b. Hence, the possibility that carriers from the source transport over Schottky barrier through thermionic emission decreases. On the other hand, when $MoSe_2$ nanomembrane is rolled up, the area exposed to air is almost doubled and high density surface states can be generated on the inner and outer surface of tube wall which can act as charge trap. The region of surface depletion layer increases with the surface charges, thus, the effective conductive region will decrease (Figure 6c). Above two factors mainly result in the current of the tubular device decreasing by half compared with that of planar device.

To understand the mechanism of the increase of photocurrent in the tubular $MoSe_2$ photodetector, numerical simulation based on finite elements methods (FEMs) was carried out. **Figure 7**a shows the simulated electromagnetic field distribution in the $MoSe_2$ microtube under the illumination of a vertical incident light (808 nm). The black annulus represents the $MoSe_2$ microtube, which is put on silicon platform. We can find that the light is trapped in the hollow core of the microtube reflecting by the local enhancement of the electromagnetic field inside the microtube, which is due to the multiple reflection. When the illumination light is applied, the light will be reflected many times inside the tubular structure.[24] At each reflection, a certain portion of the incident light will be absorbed. Hence, in addition to the incident light outside the tube, the light passing through the $MoSe_2$ membrane into the hollow core would be partly absorbed through multiple reflection, which could lead to the enhancement of light absorption. Moreover,

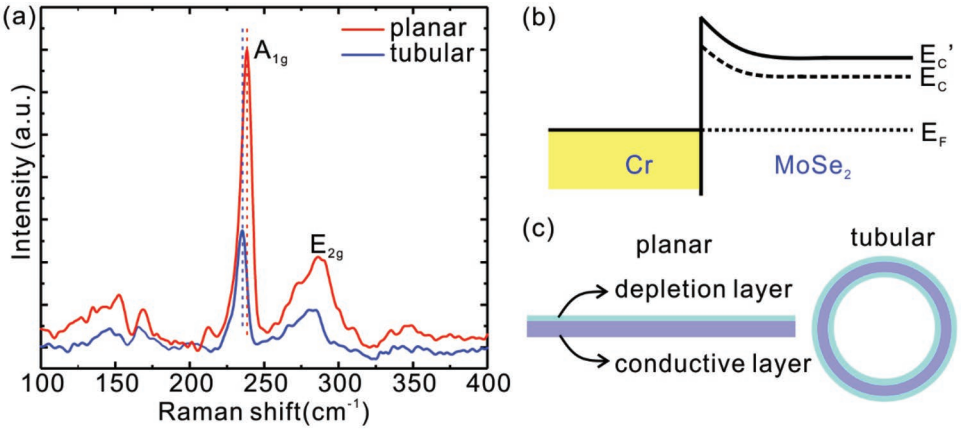

Figure 6. a) Raman spectra of $MoSe_2$ nanomembrane before (red line) and after (blue line) the rolling-up process. b) Schematic energy band diagram of the $MoSe_2$ devices (E_c': tubular; E_c: planar). c) Schematic illustration of the depletion layer in $MoSe_2$ nanomembrane before and after rolling-up process.

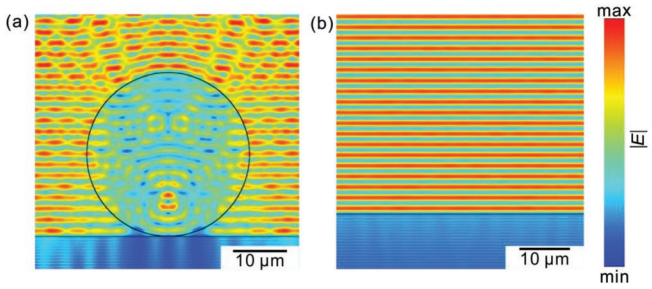

Figure 7. a) Simulation of electromagnetic field distribution in the $MoSe_2$ microtube under the illumination of a vertical incident light (808 nm). The black annulus represents $MoSe_2$ membrane. b) Simulation of electromagnetic field distribution around flat $MoSe_2$ membrane. The black line represents $MoSe_2$ membrane. (The scale bar ranges of the two images are the same.)

in contrast to tubular photodetector, the absorption enhancement phenomenon benefiting from the tubular geometry does not exist in the case of planar device. The light passing through $MoSe_2$ nanomembrane would transmit along the substrate as shown in Figure 7b and would not be reabsorbed. Simulation parameters in the planar case were set the same as in Figure 7a, except that the structure of $MoSe_2$ layer was set as rectangle instead of annulus. The comparison of the two cases illustrates that the enhanced absorption is on account of multiple reflection arising from the tubular structure, which could bring about the increase of photogenic carriers. Thus, the photocurrent in the tubular device would increase compared with the planar one.

In conclusion, $MoSe_2$ tubular photodetector was realized via self-rolled-up technology with a clear design in which Cr and Pt were deposited on top to generate strain gradient and serve as electrodes. The tubular photodetector exhibits excellent detection performance such as high photosensitivity and photoresponsivity compared with the corresponding planar device, which is on account of enhanced optical absorption, higher surface states density and bandgap modification resulting from the tubular geometry. Such rolled-up tubular photodetector has great potential for integration of 3D optoelectronics and may be applied in wide angle detection because of the symmetry in the plane perpendicular to the axis of the tube. The fabrication technique proposed in this work can be applied in the fabrication of 3D tubular photoelectronic devices based on other 2D materials such as MoS_2, WS_2 and black phosphorus.

Experimental Section

Device Fabrication: First, a layer of photoresist (AZ5214) was spin-coated on the top of $MoSe_2$ nanomembrane at 600 rpm for 6 s and 3500 rpm for 30 s. Then, the samples were baked on a hot plate at 90 °C for 90 s. Laser direct writer (uPG501) was applied to expose predesigned pattern and samples were immersed in gel developer (Tetramethylammonium hydroxide, TMAH) for about 45 s. The corrosion window was realized by etching away the exposed $MoSe_2$ layer via RIE (Sirus T2) in a SF_6 atmosphere. The parameters of the etching process were as follows: the gas flow of SF_6 was 20 sccm, the reaction pressure was 50 mTorr, and the radio frequency (RF) power was 100 W. After dissolving the photoresist in ethanol solution, the second photolithography was performed to define the area of the channel and electrodes. Afterward, the electrode layer was deposited on the $MoSe_2$ membrane by e-beam evaporation (TSV70, Tenstar) under the following conditions: cavity temperature of 25 °C, vacuum pressure of 10^{-6} mbar. Chromium (Cr) layer was deposited with the thickness of 20 nm at a deposition rate of 1 Å s^{-1}. 5 nm platinum (Pt) layer was deposited at a rate of 0.05 Å s^{-1}. After that, the sample was immersed in the 40% HF solution to selectively remove the SiO_2 sacrificial layer. SiO_2 will be selectively etched starting from the corrosion window and the $MoSe_2$/Cr/Pt layer will get released from the substrate gradually. As a result, microtubes were formed during the strain redistribution process. Finally, the sample was transferred into critical point dryer (CPD, Tousimis Autosamdri-815B) to be dried via CO_2 critical point method to avoid the collapse of the 3D tubular structure.

Scanning Electron Microscopy: SEM images of rolled-up $MoSe_2$ microtubes were measured by field emission scanning electron microscope (Zeiss Sigma) with a 5 kV working voltage.

Micro-Raman Measurement: The Raman spectroscopy was measured by a Raman spectroscope (HR800, Horiba) at an excitation wavelength of 514 nm. The laser beam was focused by a 100× objective and the laser spot size was about 1 μm.

Electrical Measurement: *I–V* characterization curves were measured by semiconductor parameter analyzer (Keithley 4200-SCS/F).

Supporting Information

Supporting Information is available from the Wiley Online Library or from the author.

Acknowledgements

This work was supported by the Natural Science Foundation of China (U1632115, 51711540298, and 61628401), the Science and Technology Commission of Shanghai Municipality (17JC1401700), the National Key Technologies R&D Program of China (2015ZX02102-003), and the China Postdoctoral Science Foundation (No. KLH2021039), the Changjiang Young Scholars Program of China and the Program of Shanghai Academic Research Leader (19XD1400600). H.J.K. and Y.J.C. acknowledge the support of the National Research Foundation of Korea (NRF) grants (NRF-2017R1C1B2004927). Part of the experimental work was carried out in Fudan Nanofabrication Laboratory.

Conflict of Interest

The authors declare no conflict of interest.

Keywords

$MoSe_2$, photosensitivity, rolling-up, tubular photodetectors

Received: May 17, 2019
Revised: August 2, 2019
Published online: September 4, 2019

[1] M. M. Furchi, D. K. Polyushkin, A. Pospischil, T. Mueller, *Nano Lett.* **2014**, *14*, 6165.
[2] Z. Yin, H. Li, H. Li, L. Jiang, Y. Shi, Y. Sun, G. Lu, Q. Zhang, X. Chen, H. Zhang, *ACS Nano* **2012**, *6*, 74.
[3] O. Lopez-Sanchez, D. Lembke, M. Kayci, A. Radenovic, A. Kis, *Nat. Nanotechnol.* **2013**, *8*, 497.

[4] J. Rhyee, J. Kwon, P. Dak, J. H. Kim, S. M. Kim, J. Park, Y. K. Hong, W. G. Song, I. Omkaram, M. A. Alam, S. Kim, *Adv. Mater.* **2016**, *28*, 2316.
[5] S. Bang, N. T. Duong, J. Lee, Y. H. Cho, H. M. Oh, H. Kim, S. J. Yun, C. Park, M. Kwon, J. Kim, J. Kim, M. S. Jeong, *Nano Lett.* **2018**, *18*, 2316.
[6] S. Kim, J. Maassen, J. Lee, S. M. Kim, G. Han, J. Kwon, S. Hong, J. Park, N. Liu, Y. C. Park, I. Omkaram, J. Rhyee, Y. K. Hong, Y. Yoon, *Adv. Mater.* **2018**, *30*, 1705542.
[7] J. Xia, X. Huang, L. Liu, M. Wang, L. Wang, B. Huang, D. Zhu, J. Li, C. Gu, X. Meng, *Nanoscale* **2014**, *6*, 8949.
[8] D. B. Velusamy, R. H. Kim, S. Cha, J. Huh, R. Khazaeinezhad, S. H. Kassani, G. Song, S. M. Cho, S. H. Cho, I. Hwang, J. Lee, K. Oh, H. Choi, C. Park, *Nat. Commun.* **2015**, *6*, 8063.
[9] F. Xia, H. Wang, D. Xiao, M. Dubey, A. Ramasubramaniam, *Nat. Photonics* **2014**, *8*, 899.
[10] N. Perea-López, A. L. Elías, A. Berkdemir, A. Castro-Beltran, H. R. Gutiérrez, S. Feng, R. Lv, T. Hayashi, F. López-Urías, S. Ghosh, B. Muchharla, S. Talapatra, H. Terrones, M. Terrones, *Adv. Funct. Mater.* **2013**, *23*, 5511.
[11] H. Tan, Y. Fan, Y. Zhou, Q. Chen, W. Xu, J. H. Warner, *ACS Nano* **2016**, *10*, 7866.
[12] Y. Xue, Y. Zhang, Y. Liu, H. Liu, J. Song, J. Sophia, J. Liu, Z. Xu, Q. Xu, Z. Wang, J. Zheng, Y. Liu, S. Li, Q. Bao, *ACS Nano* **2016**, *10*, 573.
[13] W. Wang, A. Klots, Y. Yang, W. Li, I. I. Kravchenko, D. P. Briggs, K. I. Bolotin, J. Valentine, *Appl. Phys. Lett.* **2015**, *106*, 181104.
[14] O. Salehzadeh, M. Djavid, N. H. Tran, I. Shih, Z. Mi, *Nano Lett.* **2015**, *15*, 5302.
[15] C. Javerzac-Galy, A. Kumar, R. D. Schilling, N. Piro, S. Khorasani, M. Barbone, I. Goykhman, J. B. Khurgin, A. C. Ferrari, T. J. Kippenberg, *Nano Lett.* **2018**, *18*, 3138.
[16] H. Wang, H. Zhen, S. Li, Y. Jing, G. Huang, Y. Mei, W. Lu, *Sci. Adv.* **2016**, *2*, e1600027.
[17] T. Deng, Z. Zhang, Y. Liu, Y. Wang, F. Su, S. Li, Y. Zhang, H. Li, H. Chen, Z. Zhao, Y. Li, Z. Liu, *Nano Lett.* **2019**, *19*, 1494.
[18] J. B. Kim, P. Kim, N. C. Pégard, S. J. Oh, C. R. Kagan, J. W. Fleischer, H. A. Stone, Y. Loo, *Nat. Photonics* **2012**, *6*, 327.
[19] Y. Mei, S. Kiravittaya, M. Benyoucef, D. J. Thurmer, T. Zander, C. Deneke, F. Cavallo, A. Rastelli, O. G. Schmidt, *Nano Lett.* **2007**, *7*, 1676.
[20] Q. Guo, G. Wang, D. Chen, G. Li, G. Huang, M. Zhang, X. Wang, Y. Mei, Z. Di, *Appl. Phys. Lett.* **2017**, *110*, 112104.
[21] Y. Mei, G. Huang, A. A. Solovev, E. B. Ureña, I. Mönch, F. Ding, T. Reindl, R. K. Y. Fu, P. K. Chu, O. G. Schmidt, *Adv. Mater.* **2008**, *20*, 4085.
[22] C. C. Bof Bufon, J. D. Cojal González, D. J. Thurmer, D. Grimm, M. Bauer, O. G. Schmidt, *Nano Lett.* **2010**, *10*, 2506.
[23] P. Zhang, J. Wang, W. Sheng, F. Wang, J. Zhang, F. Zhu, X. Zhuang, R. Jordan, O. G. Schmidt, X. Feng, *Energy Environ. Sci.* **2018**, *11*, 1717.
[24] D. R. Kazanov, A. V. Poshakinskiy, V. Yu. Davydov, A. N. Smirnov, I. A. Eliseyev, D. A. Kirilenko, M. Remškar, S. Fathipour, A. Mintairov, A. Seabaugh, *Appl. Phys. Lett.* **2018**, *113*, 101106.
[25] V. A. Bolaños Quiñones, L. Ma, S. Li, M. Jorgensen, S. Kiravittaya, O. G. Schmidt, *Opt. Lett.* **2012**, *37*, 4284.
[26] G. Huang, V. A. Bolaños Quiñones, F. Ding, S. Kiravittaya, Y. Mei, O. G. Schmidt, *ACS Nano* **2010**, *4*, 3123.
[27] Z. Tian, L. Zhang, Y. Fang, B. Xu, S. Tang, N. Hu, Z. An, Z. Chen, Y. Mei, *Adv. Mater.* **2017**, *29*, 1604572.
[28] B. Xu, Z. Tian, J. Wang, H. Han, T. Lee, Y. Mei, *Sci. Adv.* **2018**, *4*, eaap8203.
[29] X. Hou, R. Pan, Q. Yu, K. Zhang, G. Huang, Y. Mei, D. W. Zhang, P. Zhou, *Small* **2019**, *15*, 1803876.
[30] A. A. Solovev, Y. Mei, E. B. Ureña, G. Huang, O. G. Schmidt, *Small* **2009**, *5*, 1688.
[31] S. J. Yang, Y. Lee, J. H. Kim, H. J. Kim, B. K. Choi, H. Y. Jeong, K. Kim, J. S. Choi, Y. J. Chang, *Curr. Appl. Phys.* **2019**, *19*, 273.
[32] S. M. Poh, S. J. R. Tan, X. Zhao, Z. Chen, I. Abdelwahab, D. Fu, H. Xu, Y. Bao, W. Zhou, K. P. Loh, *Adv. Mater.* **2017**, *29*, 1605641.
[33] X. Cui, Z. Kong, E. Gao, D. Huang, Y. Hao, H. Shen, C. Di, Z. Xu, J. Zheng, D. Zhu, *Nat. Commun.* **2018**, *9*, 1301.
[34] X. Fang, P. Wei, L. Wang, X. Wang, B. Chen, Q. He, Q. Yue, J. Zhang, W. Zhao, J. Wang, G. Lu, H. Zhang, W. Huang, X. Huang, H. Li, *ACS Appl. Mater. Interfaces* **2018**, *10*, 13011.
[35] Z. Tian, B. Xu, B. Hsu, L. Stan, Z. Yang, Y. Mei, *Nano Lett.* **2018**, *18*, 3017.
[36] S. B. Desai, G. Seol, J. S. Kang, H. Fang, C. Battaglia, R. Kapadia, J. W. Ager, J. Guo, A. Javey, *Nano Lett.* **2014**, *14*, 4592.
[37] Y. Sun, D. Wang, Z. Shuai, *J. Phys. Chem. C* **2016**, *120*, 21866.
[38] T. Shen, A. V. Penumatcha, J. Appenzeller, *ACS Nano* **2016**, *10*, 4712.
[39] M. Grundmann, *Appl. Phys. Lett.* **2003**, *83*, 2444.
[40] F. Pezzoli, E. Grilli, M. Guzzi, S. Sanguinetti, D. Chrastina, G. Isella, H. von Känel, E. Wintersberger, J. Stangl, G. Bauer, *Mater. Sci. Semicond. Process.* **2006**, *9*, 541.
[41] A. Castellanos-Gomez, R. Roldán, E. Cappelluti, M. Buscema, F. Guinea, H. S. J. van der Zant, G. A. Steele, *Nano Lett.* **2013**, *13*, 5361.
[42] T. M. G. Mohiuddin, A. Lombardo, R. R. Nair, A. Bonetti, G. Savini, R. Jalil, N. Bonini, D. M. Basko, C. Galiotis, N. Marzari, K. S. Novoselov, A. K. Geim, A. C. Ferrari, *Phys. Rev. B* **2009**, *79*, 205433.
[43] C. Rice, R. J. Young, R. Zan, U. Bangert, D. Wolverson, T. Georgiou, R. Jalil, K. S. Novoselov, *Phys. Rev. B* **2013**, *87*, 081307.
[44] S. Horzum, H. Sahin, S. Cahangirov, P. Cudazzo, A. Rubio, T. Serin, F. M. Peeters, *Phys. Rev. B* **2013**, *87*, 125415.